University of Nebraska - Lincoln
DigitalCommons@University of Nebraska - Lincoln

Xiaoshan Xu Papers | Research Papers in Physics and Astronomy

2018

A brief review of ferroelectric control of magnetoresistance in organic spin valves

Xiaoshan Xu
University of Nebraska-Lincoln, xiaoshan.xu@unl.edu

Follow this and additional works at: https://digitalcommons.unl.edu/physicsxu

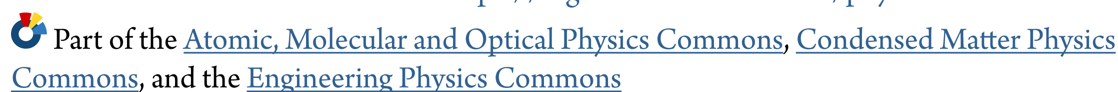
Part of the Atomic, Molecular and Optical Physics Commons, Condensed Matter Physics Commons, and the Engineering Physics Commons

Xu, Xiaoshan, "A brief review of ferroelectric control of magnetoresistance in organic spin valves" (2018). *Xiaoshan Xu Papers*. 11.
https://digitalcommons.unl.edu/physicsxu/11

This Article is brought to you for free and open access by the Research Papers in Physics and Astronomy at DigitalCommons@University of Nebraska - Lincoln. It has been accepted for inclusion in Xiaoshan Xu Papers by an authorized administrator of DigitalCommons@University of Nebraska - Lincoln.

J Materiomics 4 (2018) 1–12

Contents lists available at ScienceDirect

J Materiomics

journal homepage: www.journals.elsevier.com/journal-of-materiomics/

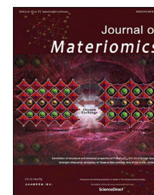

A brief review of ferroelectric control of magnetoresistance in organic spin valves

Xiaoshan Xu

Department of Physics and Astronomy, Nebraska Center for Materials and Nanoscience, University of Nebraska, Lincoln, NE 68588, USA

A R T I C L E I N F O

Article history:
Received 16 September 2017
Received in revised form
8 November 2017
Accepted 11 November 2017
Available online 13 November 2017

Keywords:
Organic spin valve
Ferroelectricity
Spinterface
Magnetoresistance

A B S T R A C T

Magnetoelectric coupling has been a trending research topic in both organic and inorganic materials and hybrids. The concept of controlling magnetism using an electric field is particularly appealing in energy efficient applications. In this spirit, ferroelectricity has been introduced to organic spin valves to manipulate the magneto transport, where the spin transport through the ferromagnet/organic spacer interfaces (spinterface) are under intensive study. The ferroelectric materials in the organic spin valves provide a knob to vary the interfacial energy alignment and the interfacial crystal structures, both are critical for the spin transport. In this review, we introduce the recent efforts of controlling magnetoresistance of organic spin valves using ferroelectricity, where the ferroelectric material is either inserted as an interfacial layer or used as a spacer material. The realization of the ferroelectric control of magneto transport in organic spin valve, advances our understanding in the spin transport through the ferromagnet/organic interface, and suggests more functionality of organic spintronic devices.

© 2018 The Chinese Ceramic Society. Production and hosting by Elsevier B.V. This is an open access article under the CC BY-NC-ND license (http://creativecommons.org/licenses/by-nc-nd/4.0/).

Contents

1. Introduction 1
2. Diffusive spin valves 3
3. Tunneling spin valves 4
4. Organic spin valves 4
5. Ferroelectric interfaces 5
6. Control of spin transport using ferroelectric interfaces 6
   6.1. Diffusive organic spin valves and interfacial energy alignment 7
   6.2. Tunneling organic spin valves and the interfacial crystal structure 9
7. Conclusion and outlook 10
   Acknowledgements 10
   References 10

1. Introduction

Giant magnetoresistance has been a successful example of nanotechnology in which transport of spin-polarized current through interfaces is manipulated in nanoscale to vary the resistance of the devices. Wide application of this effect, such as in the read heads of the hard disks for much larger information density, has been realized; the fundamental research was awarded Nobel prizes in 2007. The concept of manipulating the spin degree of freedom of electrons to control the electrical transport, has now evolved into a large active field of research and technology, i.e. spintronics, with emphasis more and more on spin transport and application potentials in information storage and processing, sensors, energy generation, etc. [1–5].

The effect of giant magnetoresistance can manifest in a trilayer junction shown in Fig. 1(a). The junction contains a non-magnetic

E-mail address: xiaoshan.xu@unl.edu.

Peer review under responsibility of The Chinese Ceramic Society.

https://doi.org/10.1016/j.jmat.2017.11.003

2352-8478/© 2018 The Chinese Ceramic Society. Production and hosting by Elsevier B.V. This is an open access article under the CC BY-NC-ND license (http://creativecommons.org/licenses/by-nc-nd/4.0/).

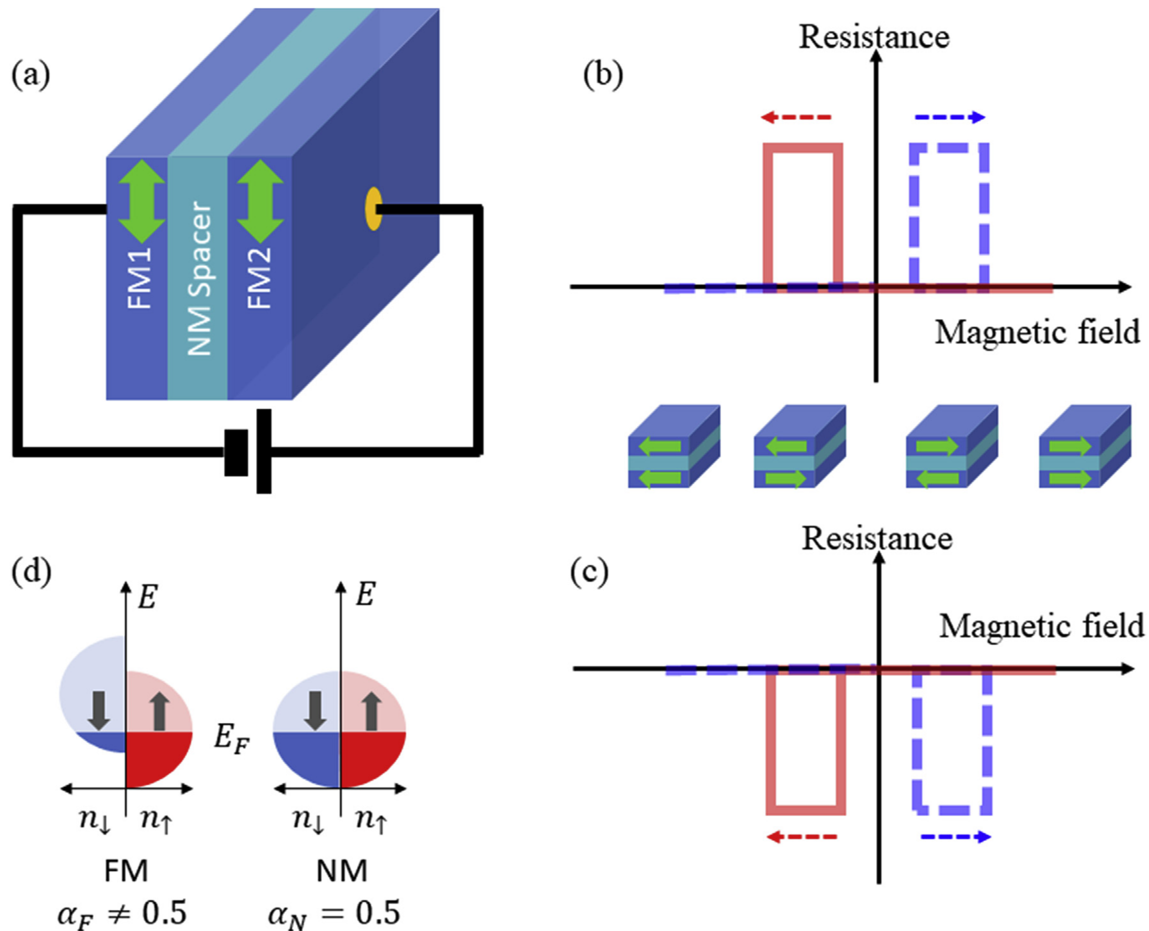

Fig. 1. (a) Schematics of an FM/NM/FM trilayer spin valve. (b) and (c) are the magnetic-field dependence of resistance of the spin valve for positive (normal) and negative (inverse) MR respectively. (d) Schematics of the electronic structure of the FM and NM materials, where $n_\uparrow$ and $n_\downarrow$ are the number of states of the up spin and down spin respectively.

(NM) spacer layer sandwiched by two ferromagnetic (FM) electrodes. Depending on the alignment of the magnetization of the two FM electrodes, the resistance of the junction changes between high and low values. The trilayer junction can then be regarded as a spin valve, in the sense that the electrical current can be turned on and off using the external magnetic field which controls the alignment of the magnetization of the two FM electrodes. Depending on the spacer materials and the thickness, three categories of spin valves are mostly studied. 1) If the spacer material is a metal, the magnetoresistance (MR) is expected to be small compared with the volume resistance [6]. Superlattice-fashioned structures were adopted to enhance MR by increasing the number of interfaces while keeping the thickness of the junction and the volume resistance constant [7–11]. In this case, the thickness of the spacer is often less than a few nanometers; the MR has to do with the indirect exchange coupling between the magnetic layers [12,13]. 2) If the spacer is a thick semiconductor, the two FM layers are magnetically decoupled and the transport through the spacer becomes diffusive. In this case, the MR hinges on spin injection, which is actually difficult for a metal/semiconductor ohmic contact. Tunneling through a barrier between the FM and the semiconductor provides a more efficient route for the spin injection [14–17]. 3) If the spacer is a thin insulator, the electrical transport is based on spin-conserved tunneling between the two electrodes. Therefore, the MR is related to the alignment of spin polarization of the initial and final states of the tunneling.

Organic spin valves are trilayer structures including organic semiconductors (OSC) or insulators as the spacer materials. The long spin life time of the organic materials [18,19] (due to the weak spin-orbit coupling in the light elements such as carbon and hydrogen), is appealing for spin transport. In addition, the flexibility, environment friendliness, and the vast chemical diversity of organic materials suggest great application potentials of organic spintronic devices. Organic spin valves generally belong to the latter two categories introduced above, where the two FM electrodes are decoupled in terms of exchange interactions [6]. The alignment of the magnetization of the two FM electrodes, can be tuned by an external magnetic field, based on their difference in magnetic coercivity. The MR has a butterfly-like shape, as illustrated in Fig. 1(b) and (c). If the resistance of the spin valve is high (low) when the magnetization of the two FM layers are antiparallel, it is called normal (inverse) or positive (negative) MR.

Encouraged by early promising results on organic spin valves [20,21], efforts on understanding the fundamental mechanism and on realizing organic spintronic devices, has been growing rapidly. However, several key issues, such as spin injection and spin polarization at the FM/organic interfaces, are still not fully understood in organic spin valves. To tackle these key issues, being able to tune the crystal structure and electronic structure at the FM/organic interfaces (spinterface [22]) appears to be critical, because the sign and magnitude of the MR is determined by the spin polarization at these interfaces, which are sensitive to the

electronic structure. The electronic structure at the FM/spacer interface is a result of coupling between that of the two materials, which is based on the crystal structure and the energy level alignment of the two materials. Ferroelectric (FE) materials, either as an interfacial material or as the spacer itself, offer tunabilities to the electronic structures at the interface, by changing the energy level alignment or the interfacial crystal structure. Besides the important role in studying fundamental mechanism, the FE controlled organic spin valves also have potential applications in multi-state information storage devices and energy efficient information processing, because the changes caused by the FE material, via switching the electrical polarization using an electric field, are non-volatile.

Here we review the topic of FE control of MR in organic spin valves as one of the frontiers of organic spintronics. Inspired by similar work in inorganic spin valves and previous efforts in tuning FM/organic interfaces [23–32], recently, a sequence of work has studied the multistates in the organic spin valves using FE materials as the spacer or as an interfacial layer [33–36]. The results confirm the critical role of energy alignment and interfacial structure in the spinterface.

The topic is reviewed as an integrated story based on the current understanding: First, we organize the fundamental principles that are necessary for understanding the topic, including the concepts and fundamental processes in the diffusive and tunneling spin valves and the specific problems in organic spin valves. The FE control of MR in organic spin valves is then presented and analyzed using these principles. The effects of FE materials on the interfaces are sorted into two categories: the electrostatic change of energy alignment and the interfacial structural change due to the polarization reversal.

2. Diffusive spin valves

A spin valve can be realized in a junction where electrical current flows diffusively, which means that the electrochemical potential of the charge carriers changes when they travel through the junction. To understand the MR of the diffusive spin valves, it is better to discuss the boundary resistance at the FM/NM interface first. In the two-current (spin up and spin down) model [37], the fundamental difference between the FM and the NM, are in the equilibrium spin polarization (α), defined as the proportion of the spin-up branch of the current, which represents the proportion of spin-up density of states at the Fermi level [Fig. 1(d)]. For the FM and NM layers, one has $\alpha_F \neq 0.5$ and $\alpha_N = 0.5$ respectively. When the spin polarized current flows from the FM layer into the NM layer, it tends to depolarize toward the equilibrium state of the NM layer. As shown in Fig. 2(a), the dynamics of the spin polarization can be modelled using the difference of electrochemical potentials of the spin-up and spin-down branch of the current, assuming no interfacial spin scattering. If we assume $\alpha_F > 0.5$ (spin up carriers are the majority), near the FM/NM interface, the electrochemical potential of the spin-up branch has to be higher than that of the spin-down branch, to drive the population from the former to the latter. This is true also on the NM side of the interface [Fig. 2(a)], indicating that the charge carriers are also spin-polarized near the interface on the NM side [Fig. 2(b)]. The spin polarization in the NM layer is referred to as the spin accumulation. In this case, the spin injection is realized by the transport of spin-aligned charge carriers through the FM/NM interface [1,5], as opposed to the spin injection by purely spin diffusion in lateral structures [38].

The mean electrochemical potential of the current is discontinuous at the interface [Fig. 2(a)], which is the origin of the boundary resistance (R_B), given as

$$\frac{1}{R_B} = \frac{1}{(\alpha_F - \alpha_N)^2}\left[\frac{\alpha_F(1-\alpha_F)}{\lambda_F/\sigma_F} + \frac{\alpha_N(1-\alpha_N)}{\lambda_N/\sigma_N}\right]$$

where λ_F and λ_N are the spin diffusion length [39,40] of the FM and NM layers respectively, σ_F and σ_N are the conductivity of the FM and NM layers respectively. The boundary resistance can also be understood in terms of the population change between the two current branches, or virtual currents. In general, the virtual currents run on both the FM side and the NM side of the interface in parallel over the distance about the spin diffusion length, as shown in Fig. 2(b). The additional resistance (R_B) of the interface due to the virtual current (change of spin polarization) is then the two resistances $R_{NB} = \frac{\lambda_N}{\sigma_N}\frac{(\alpha_F-\alpha_N)^2}{\alpha_N(1-\alpha_N)}$ and $R_{FB} = \frac{\lambda_F}{\sigma_F}\frac{(\alpha_F-\alpha_N)^2}{\alpha_F(1-\alpha_F)}$ in parallel. Notice that if $\alpha_F = 1$ (half metal FM), only R_{NB} contributes to the boundary resistance. Accordingly, the change of spin polarization of the charge carriers occurs only in the NM layer and the spin injection is 100%.

In a FM/NM/FM trilayer structure, if the NM layer is thin enough compared with λ_N, the spin polarization at the two FM/NM interfaces, interferes [41]. If the spin polarizations of the two FM layers are along the same direction [Fig. 2(c) and (d)], the current may not have to totally depolarize at one interface before it is polarized at the other interface. The difference between the electrochemical potentials of the two current branches is then smaller; the discontinuity of the mean electrochemical potential and the boundary resistance, which both come from the change of spin polarization, are reduced compared with those when the spin polarizations of the two FM layers are along the opposite directions [Fig. 2(e) and (f)]. If the thickness of the NM layer d is much smaller than λ_N ($\frac{d}{\Lambda_N} \ll 1$) and the two FM materials are identical, one has $R_B^{\uparrow\uparrow} = \frac{\alpha_{F1}(\alpha_{F1}-\alpha_N)}{2\alpha_N(1-\alpha_N)}\frac{\lambda_N}{\sigma_N}\frac{d}{\Lambda_N}$ and $R_B^{\uparrow\downarrow} = \frac{(2\alpha_{F1}-1)^2}{2\alpha_{F1}(1-\alpha_{F1})}\frac{\lambda_{F1}}{\sigma_{F1}}$ for the parallel and antiparallel alignment respectively; hence $R_B^{\uparrow\downarrow} \gg R_B^{\uparrow\uparrow}$ This change of boundary resistance due to the change of relative alignment of the spin polarization of the two FM layers, is the mechanism of the giant magnetoresistance in the classical two-current model.

Notice that it is alignment between the spin polarizations of the charge carriers of the two FM layers instead of that between the magnetization of the two FM layers, that determines the MR. The MR sign of a spin valve can be analyzed in terms of quantum mechanical description of the spin polarization, defined as $P = \frac{n_M - n_m}{n_M + n_m}$, where n_M and n_m are the number of states of the majority spin and minority spin respectively of the states of certain energy. For typical metallic ferromagnets like Co, at the Fermi level, most states have the minority spin, corresponding to $P < 0$ [42]. For the oxide conductor $La_{0.7}Sr_{0.3}MnO_3$ (LSMO), which is often used as an FM electrode, the states at Fermi level corresponds to $P > 0$ [43]. To analyze the MR sign, one defines the interfacial spin polarization P_1^* for the carrier injection as the P of the initial states. Similarly, the interfacial spin polarization of the carrier collection P_2^* is the P of the final states. The MR sign can be predicted from $P_1^* P_2^*$, where positive (negative) values of the product correspond to normal (inverse) MR. If the spacer is a non-magnetic metal, interfacial spin corresponds to the spin polarization at the Fermi level of the FM materials. If the spacer is a semiconductor, the interfacial spin polarization depends on the detailed coupling between the electronic structures of the FM and spacer material at the interfaces.

The MR of the trilayer diffusive spin valve comes from the change of boundary resistance. The absolute value of the boundary resistance is on the order of the resistance of the junction materials (two FM layers and one NM layer) over the length scale of the spin diffusion length, which may be small compared with the volume resistance in the all-metal junctions. Hence, the MR is not expected to be very large in the all-metal trilayer diffusive spin valves. Unfortunately, the MR cannot be enhanced simply by replacing the

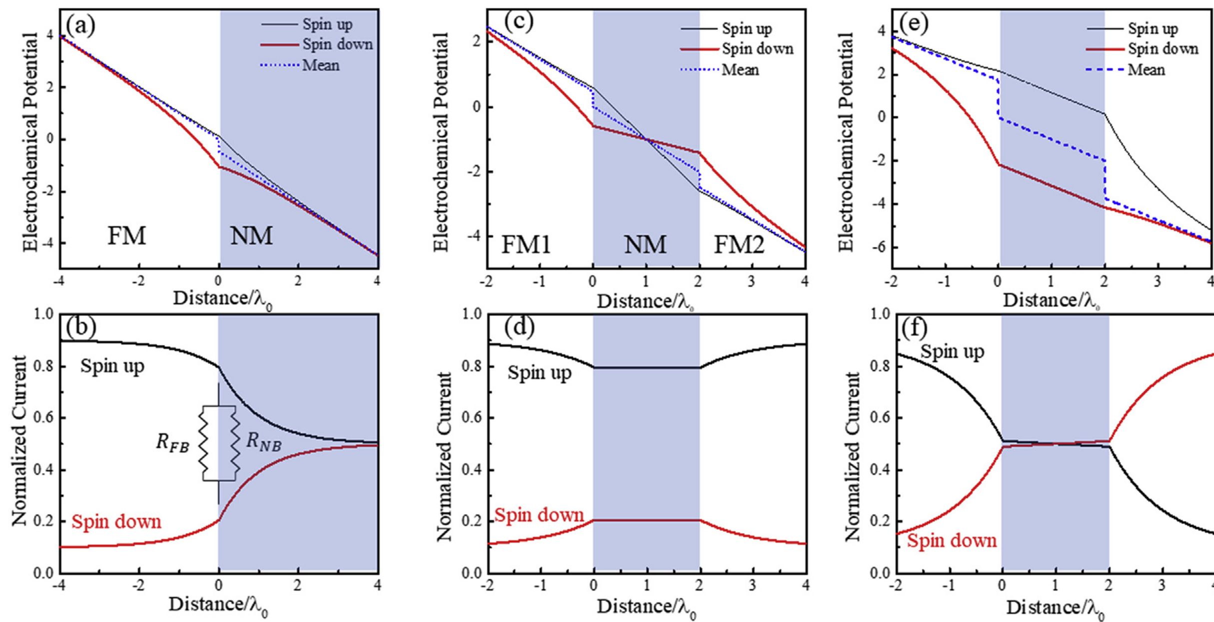

Fig. 2. Calculated spatial dependence of the electrochemical potential and the normalized current in the two-current model. (a) and (b) are near a FM/NM interface. (c) and (d) are for a trilayer spin valve when the spin polarization of the two FM layers are aligned ($\alpha_{FM1} > 0.5, \alpha_{FM2} > 0.5$). (e) and (f) are for a trilayer spin valve when the spin polarization of the two FM layers are anti-aligned ($\alpha_{FM1} > 0.5, \alpha_{FM2} < 0.5$). The calculation assumes: $\lambda_{F1} = \lambda_{F2} = \lambda_0$, $\lambda_N \gg \lambda_0$, and $d = 2\lambda_0$, where λ_0 is a length scale.

spacer with materials of much larger resistivity. According to Eq. (1), the total boundary resistance is the resistance of the FM and NM channels in parallel. So, increasing only the NM resistance does not change the total boundary resistance significantly. In fact, the large NM resistance reduces the spin injection into the NM layer, i.e. the depolarization of the spin current occurs mostly in the FM layer because the FM channel has much smaller resistance. Hence, the two FM/NM interfaces are decoupled, and little MR is expected. This is the famous impedance-mismatch problem [44].

3. Tunneling spin valves

The impedance-mismatch problem is absent in the tunneling spin valves. When the NM layer is insulating and thin enough, the mechanism of electrical conduction becomes quantum tunneling, in which the spin states of the carriers are conserved. The transition from initial states in FM1 to final states in FM2, depends on the relative spin polarization of these states. Therefore, one may observe resistance change when the relative alignment of the magnetization of the two FM electrodes is manipulated by the external field.

Similar to that in the diffusive spin valve, it is the spin polarization of the initial and final states that matters for the MR sign. Since the tunneling resistance is much larger than the resistance of the electrodes, the estimation of MR may ignore the volume-resistance contribution from the electrodes. Hence, in the Julliere's model [45], MR is predicted as $\frac{2P_1P_2}{1-P_1P_2}$, where P_1 and P_2 are the spin polarization of the initial and final states of the tunneling in the two FM electrodes. According to this model, much larger MR is possible compared with that in the diffusive spin valves. Indeed, the tunneling MR up to 600% has been reported by Ikeda et al., in CoFeB/MgO/CoFeB spin valves at 300 K [46].

Under bias voltage, the initial and final states in FM1 and FM2 may shift with respect to the Fermi level. Since the spin polarization of states at different energy levels may be different, the MR may change with the bias voltage. De Teresa et al. studied LSMO/STO/Co tunneling spin valve [42], where STO stands for $SrTiO_3$. At low bias voltage, the negative P in Co and the positive P in LSMO results in an inverse MR. At higher bias, different part of the states of the Co participate in the tunneling, significantly different MR, both in magnitude and in sign, was observed. The bias-voltage dependence of the MR reflects the spin density of states of Co.

The electronic structure of the tunneling barrier (spacer) also plays an important role in the tunneling MR. In the case of Co, the spin polarization P of the s and d states at the Fermi level are positive and negative respectively [42,47], while in LSMO, the Fermi level is only occupied by the d states, which has a positive spin polarization P [43]. If the barrier is Al_2O_3, the tunneling of s electrons from and to Co Fermi level is favored. If the barrier is STO, the d carriers in Co is more involved in the tunneling [47].

4. Organic spin valves

In an organic spin valve, the spacer is an organic insulator or semiconductor. One can construct organic tunneling spin valve using a thin organic spacers [48–53]. For example, Barraud et al. reported a 300% MR in LSMO/Alq_3/Co tunneling spin valve at 2 K [54], where Alq_3 stands for tris-(8-hydroxyquinoline) aluminum; Santos et al. reported an 8% tunneling MR in a similar junction at room temperature [48], both in tunneling organic spin valves.

If the organic layer is too thick for the charge carriers to tunnel, diffusive conduction through the junction is expected. Since the organic insulator and semiconductors all have much larger resistance than that of the electrodes, the impedance mismatch problem discussed above could minimize the MR. Surprisingly, a sizable MR (~10%) have been repeatedly observed in the organic spin valves using LSMO as one of the FM electrodes [20,55–62]. To resolve the controversy, whether spin injection (spin polarized charge carriers in the organic spacer) occurs, has been intensively tested.

Widely accepted demonstration of spin injection employs the Hanle effect [38,63–67]. To show the Hanle effect in a trilayer spin valve, a magnetic field perpendicular to the magnetization of the FM electrodes is applied. The spin of the charge carriers is expected to precess due to the magnetic field when they travel through the

spacer. The period of the precession is inversely proportional to the external magnetic field. Therefore, the spin polarization of the charge carriers after going through the spacer can be tuned using the magnetic field; the resistance of the junction oscillates with respect to the transverse magnetic field [68–71]. Hanle effect has been successfully employed to demonstrate spin injection into inorganic semiconductors using the hot electron injection [68–74]. On the other hand, similar oscillatory magnetic-field dependence of resistance has not been observed in organic spin valves by flowing charge carriers [75], despite that fact that the spin injection has been demonstrated by muon spin resonance [76,77] and two-photon photoemission [78]. Nevertheless, the spin injection into OSCs, pumped by the ferromagnetic resonance and detected by the inverse spin Hall effect, has been demonstrated, indicating spin diffusion and precession in the OSCs, which is essential for the Hanle effect [79].

Although the issue certainly has not been settled, several possibilities may reconcile the observed spin injection and apparent impedance mismatch. One possibility is that, in the LSMO/Alq_3/Co junctions, the spin injection can be greatly enhanced due to the high spin polarization of charge carriers in LSMO (half metal) [20,21,43,55–60,80,81]. Indeed, the MR of the NiFe/Alq_3/FeCo junction is much smaller than that in the LSMO/Alq_3/Co junctions [76,82,83]. Another possibility is that the injection of spin polarized current into the organic spacer comes from tunneling through a barrier between the FM electrode and the spacer, before the current transports diffusively in the spacer [14,15] [84].

Compared with inorganic spin valves, the spin transport through organic spin valves mostly has a disordered nature with small diffusion length [85–87], which may affect the measurement of Hanle effect. Nevertheless, the Hanle effect has been observed in non-local structure of inorganic junctions, where the spin transport is totally by diffusion [38]. Therefore, it was speculated that the absence of oscillatory magnetic-field dependence of resistance is due to the significant discrepancy between the time scale of spin transport and that of the charge transport[75]. Otherwise, if one assumes that the spin and charge travel in the same speed, a unreasonable mobility for the charge transport is needed to explain the experimental observation [75]. Therefore, model with decoupled charge and spin transport has been proposed, in which the spin transport relies on exchange interactions [88,89]. Experimental evidence of exchange-mediated spin transport was later reported [90].

One practical concern for organic spin valves of vertical transport is the sharpness of the interface between the organic layer and the top electrode. Since most top electrodes are deposited on the organic spacer using vapor deposition, inter-diffusion and reaction between the spacer and the electrode, are likely to occur. Various methods have been introduced to minimize the effect of the imperfect interface, including the deposition of a buffer layer [91] between the organic spacer and the electrode and the deposition of the electrode in the form of nanoparticles instead of atomic vapor [58].

To alleviate the problem of impedance mismatch and interfacial diffusion and reaction, all-organic spin valves have been developed using organic magnetic semiconductors as the electrodes [92]. Although clear magnetoresistance has been observed, the magnitude is small compared with other spin valves, suggesting the need for better organic magnetic electrodes as well as optimization of the interfaces.

5. Ferroelectric interfaces

Ferroelectric materials are crystalline materials that exhibit spontaneous electrical polarizations switchable by an external electric field [93]. The electric polarization originates from the displacement of positive and negative charge centers, which is allowed only when the crystal structure lacks inversion symmetry. Therefore, the switching of polarizations of FE materials involves both displacement of atoms and the corresponding shift of charges; both can be employed in active control of interfacial properties.

The existence of an electric dipole, i.e. separated positive and negative charges, generates uneven electric potential in space. As illustrated in Fig. 3(a), in an FE film where polarization is pointing perpendicular to the film plane, the electric potential undergoes a rapid change across the film due to the electric field inside the material. The surface potentials are $\phi_{S\pm} = \pm\frac{\sigma_P}{2\varepsilon\varepsilon_0}d$, where σ_P is the surface charge of the FE, ε_0 and ε are the vacuum dielectric constant and the relative dielectric constant of the FE respectively, and d is the thickness of the FE layer [94]. Outside the FE film, the potential decays with a length scale much larger than the film thickness. When another material is in contact with an FE material, its charge distribution and the electrochemical potentials at the interface will be affected. For example, at an FE/metal interface, the charge in the metal accumulates to screen the charge of the FE and cancel the electric field. Fig. 4(b) illustrates the charge distribution of a metal/FE/metal junction. Using the Thomas-Fermi model of screening and assuming the two metals are electrically shorted, one obtains the electric potentials on the two metal sides that decay exponentially:

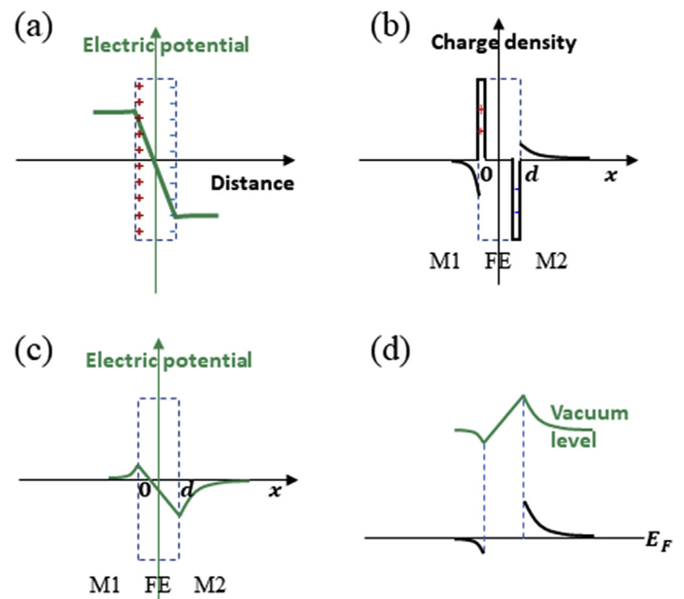

Fig. 3. (a) Spatial dependence of the electric potential caused by a ferroelectric film (indicated using the charge distribution). (b) and (c) are the charge distribution and the vacuum electric potential of a metal/FE/metal junction. (d) Energy level bending and shift at the metal/FE/metal junction. The lower curve represents the metal states that are at the Fermi energy far away from the FE.

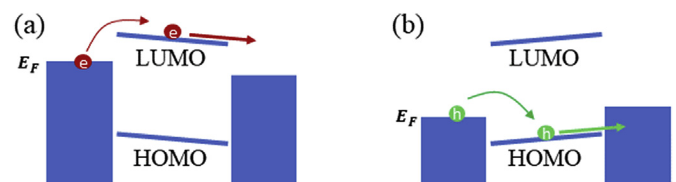

Fig. 4. The schematics of the charge transport across a metal/OSC/metal junction. (a) When the Fermi energy of the metal is close to the LUMO of OSC, electron transport is favored. (b) When the Fermi energy of the metal is close to the HOMO of OSC, hole transport is favored.

$\phi_1 = \frac{\sigma_s \delta_1}{\varepsilon_0} e^{\frac{x}{\delta_1}}$ and $\phi_2 = -\frac{\sigma_s \delta_2}{\varepsilon_0} e^{-\frac{x-d}{\delta_2}}$, where δ_1 and δ_2 are the screening lengths in the metal 1 (M1) and metal 2 (M2) respectively, and $\sigma_s = \frac{d\sigma_P}{\varepsilon(\delta_1+\delta_2)+d}$ is the screening charge [25,94]. When the screening length of the metal is much larger than the thickness of the FE, one has $\sigma_s \ll \sigma_P$ and the potentials at the FE/metal interfaces are basically the same as that of the FE surface potential. When the screening length is much smaller than that of the thickness of FE, one has $\sigma_s \approx \sigma_P$ and the potential at the FE/metal is greatly reduces. For “good” metallic materials like Co and Fe, the screening length is less than an angstrom, which suggests a complete screening of charge, or zero potential at the interface.

The screening at the two FM/metal interfaces can be different and cause asymmetric electric potentials. As shown in Fig. 4(d), the larger screening length results in smaller screening charge and larger interfacial potential. The electric potential in Fig. 4(c) determines the vacuum potential of electrons in the junction materials. The uneven vacuum potential causes the bending and shift of energy bands in the materials in contact with the FE [Fig. 4(d)], similar to that in the Schottky contact between a metal and a semiconductor [95,96]. In the case of Schottky contact, the accumulation of charge at the interface is the response to the chemical potential (Fermi energy) difference [95,96], while it is the response to the electrostatic potential difference that causes the charge accumulation at the FE/metal interface. Although it is common for the interface of two materials of different work functions to have charge accumulation and interfacial dipoles [97,98], the FE materials enables the tunability of the electrochemical potentials at the interface using an external electric field in a nonvolatile fashion.

When the two FM electrodes can both screen well, the effect of the FE polarization on the vacuum potential and energy alignment is minimized. In this case, the atomic displacement of the FE can alter the crystal structure at the FE/FM interface, causing the subtle changes of electronic structures at the interface. For example, an orbital reconstruction has been reported on the $BaTiO_3$/LSMO interface when the polarization of $BaTiO_3$ was switched [32]. A change of interfacial magnetization was also observed on this FE/FM interface by reversing the FE polarization [99].

6. Control of spin transport using ferroelectric interfaces

We have discussed two types of spin valves (diffusive and tunneling) and two effects of polarization reversal on the FE/FM interfaces (electrostatic and crystal structural). One can imagine four different scenarios in controlling the spin transport using ferroelectric interfaces. Not all the scenarios have been experimentally observed, however.

For inorganic spin valves, tunneling MR modified by the change of the FE/FM interfacial structure due to the FE polarization reversal, has been the most studied mechanism of FE control of MR, as seen from the growing interests in inorganic multiferroic tunnel junctions [24,100,101]. As mentioned above, in the tunneling spin valves, the coupling between the barrier and the FM electrode in electronic structures may affect the interfacial spin polarization significantly. If the two FM electrodes are different, the FE polarization reversal and the corresponding atomic displacements, may change the interfacial spin polarization and the MR, as has been reported experimentally [24,100,101]. For example, in the Co/PZT/LSMO tunnel junction (PZT stands for $PbZr_{0.2}Ti_{0.8}O_3$), four resistance states have been observed, depending on both the electric polarization of PZT and the magnetic alignment between Co and LSMO. This result can be explained using the change of electronic structure at the Co/PZT interface caused by the interfacial structural change after the polarization of PZT is reversed.

For organic spin valves, predictions of FE control of MR have been made in tunneling spin valves [36,102]. The mechanisms include both electrostatic shift of energy levels and the change of interfacial crystal structure. For example, tunneling electroresistance (ER) and change of MR have been predicted in organic spin valve Co/PVDF/O/Co [102], where PDVF stands for poly(-vinylidene fluoride) [103]. The asymmetric screening length at the two sides of the junction, small for the metal Co and high for the cobalt oxide, enables substantial change of electronic structure in terms of band shift and change of interfacial spin polarization. Therefore, the junction resistance can be tuned by both the electric and the magnetic fields. A four-state resistance has also been

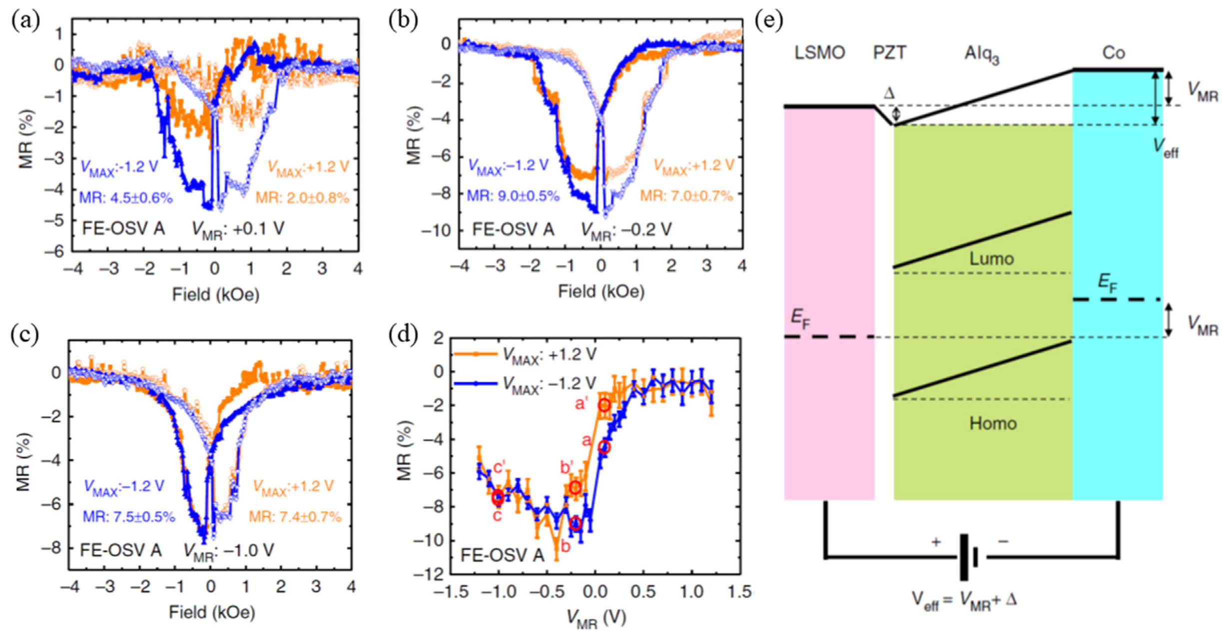

Fig. 5. MR of the LSMO/PZT/Alq_3/Co junction. (a)–(c) are the MR measured at 0.1, −0.2, and −1.0 V respectively when a 1.2 or a −1.2 V initial voltage is applied. (d) Is the MR as a function of measurement voltage (V_{MR}) when a 1.2 or a −1.2 V initial voltage is applied. (e) Is the schematic diagram indicating that the shift of vacuum level and the change of effective voltage on the OSC caused by the FE dipole of PZT.

predicted in organic spin valve Co/PVDF/Fe/Co, where the reversal of polarization switches the interfacial structure between Fe:H-C-F:Co and Fe:F-C-H:Co, which causes the change of spin polarizations and the MR [36].

Experimentally, the predicted FE control of MR in tunneling organic spin valves has been confirmed recently [33,34]. In addition, the FE control of MR has also been realized in diffusive organic spin valves; the mechanism appears to be the electrostatic shift of energy levels by the change of the FE polarizations. Next, we analyze these results based on the fundamental principles discussed above.

6.1. Diffusive organic spin valves and interfacial energy alignment

In a diffusive spin valve using an OSC spacer, the energy alignment at the FM/NM interfaces plays an important role in the spin transport, by affecting the interfacial spin polarization P^*. First, the alignment between the Fermi level of the metals and the molecular energy levels of the OSC, determines the charge carrier type in the electric transport through the junction. As shown in Fig. 5(a), if the metal Fermi energy is closer to the lowest unoccupied molecular orbital (LUMO), the main charge carriers are electrons. If the metal Fermi energy is closer to the highest occupied molecular orbital (HOMO), the main charge carriers are holes. Second, in the carrier collection process, energy level of the final states in the metal is determined by the energy level of carriers in the OSC. For an FM material, because the spin polarization of states at different energy levels may be different, the spin polarization of carrier collection P^* is likely different for different carrier types and different energy alignment between the OSC and the FM.

The alignment between the metal Fermi energy and the HOMO/LUMO of OSC can be adjusted by using metals of different work functions as the electrodes. This effect has been studied by comparing the magneto transport of the Co/Alq_3/NiFe junction and the Co/Ca/Alq_3/Ca/NiFe junction [26]. For Fe, Co, and Ni, the work functions are large (5.0 eV [104]) and the Fermi energy is closer to the HOMO of Alq_3. So, the hole transport is expected in the Co/Alq_3/NiFe junction. The work function Ca is much smaller (2.9 eV [104]) and the Fermi energy is closer to the LUMO of Alq_3. So, the transport of electrons through LUMO of Alq_3 is expected. Experiments show significantly smaller resistance in the Co/Ca/Alq_3/Ca/NiFe junction. In addition, a much larger MR with a reversed sign in Co/Ca/Alq_3/Ca/NiFe was observed, indicating a change of charge carrier type between these two junctions.

The energy alignment between the metal and the OSC can also be manipulated by inserting a dipolar layer between the metal electrode and the OSC. Using LiF as the dipolar materials, Schultz et al. studied the magneto transport in the NiFe/Alq_3/FeCo and the

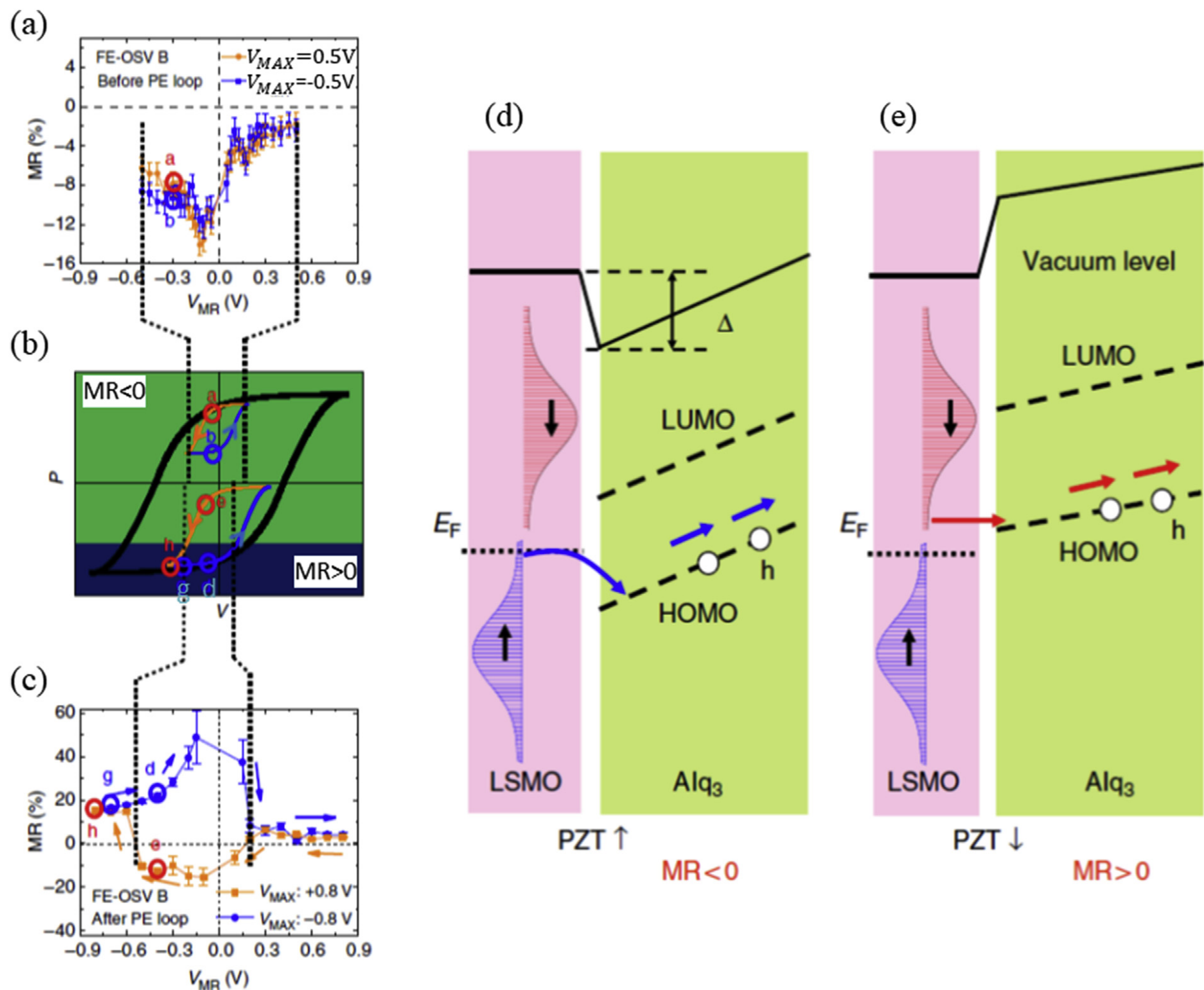

Fig. 6. (a) MR as a function of measurement voltage (V_{MR}) when a 0.5 or a −0.5 V initial voltage is applied. (b) Schematics of the polarization-voltage hysteresis loop of PZT and the minor loops. (c) MR as a function of measurement voltage (V_{MR}) when a 0.8 or a −0.8 V initial voltage is applied. Before the measurement, the PZT was poled to negative saturation polarization. (d) and (e) are the energy level alignment of the LSMO/PZT/Alq_3 interface when PZT polarization is pointing toward Alq_3 and toward LSMO respectively.

NiFe/LiF/Alq_3/FeCo junctions [76]. The spin polarization in the Alq_3 was measured using muon spin resonance. It was found that, by inserting the LiF layer (1 nm), the spin polarization of the carrier collection from Alq_3 to NiFe electrode changes from negative to positive. Consequentially, the sign of the MR is also reversed: while the NiFe/Alq_3/FeCo junction shows a negative MR, the NiFe/LiF/Alq_3/FeCo shows a positive MR. These observations are consistent with the existence of a large interfacial dipole due to the insertion of LiF layer. Since Alq_3 is a semiconductor with a screening length much longer than the spacer thickness, the vacuum potential generated by the LiF dipole is maintained and shifts the HOMO/LUMO of Alq_3 at the interface. In the NiFe/Alq_3/FeCo junction, the collected holes from Alq_3 HOMO goes into an energy level with mostly spin minority states ($P^*<0$). In contrast, due to the shift of HOMO downwards by the LiF layer, the collected holes from Alq_3 HOMO may go into an energy level with mostly spin majority states ($P^*>0$). This change of spin polarization of carrier collection leads to the change of MR sign.

If the dipole inserted between the FM electrode and the OSC comes from an FE material, the effect on the magneto transport is tunable by an electric field, due to the switchability of the FE dipole. This effect has been studied by Sun et al. in LSMO/PZT/Alq_3/Co junctions [35], where PZT is an oxide FE material with a large electric polarization (~80 μC/cm^{-2}) [105]. It was found that the MR depends on the initial voltage applied on the junction. The bias dependence of the MR, or the $MR(V_{MR})$ function, was used to gauge the effect of the initial voltage, where V_{MR} is the measurement voltage of the MR. The results show that by applying a positive (negative) initial voltage V_{MAX} that is larger than the measurement voltage V_{MR}, the $MR(V_{MR})$ function of the LSMO/PZT/Alq_3/Co junction with as-grown PZT, shifts toward the negative (positive) voltage directions [Fig. 5 (a)-(d)]; the sign of MR is always negative. The shift become larger when the initial voltage V_{MAX} is larger. More importantly, this shift of the $MR(V_{MR})$ function could not be observed in several control junctions, including LSMO/Alq_3/Co, LSMO/STO/Alq_3/Co, and LSMO/PZT/Co. These observations are consistent with the presence of an interfacial dipole due to the PZT layer between LSMO and Alq_3. Since Alq_3 is a semiconductor with poor screening ability, the dipole from PZT is maintained and causes a shift of vacuum potential (Δ) of Alq_3; the effective voltage applied on Alq_3 becomes $V_{eff} = V_{MR} + \Delta$. The initial voltage V_{MAX} changes the dipole and shifts the vacuum potential. Positive (negative) V_{MAX} makes Δ more positive (negative), corresponding to the shift of $MR(V_{MR})$ function toward the negative (positive) V_{MR} direction. It is understandable that the shift of the $MR(V_{MR})$ function is not observed in the LSMO/Alq_3/Co and LSMO/STO/Alq_3/Co junctions, because there is no interfacial FE dipole. For the LSMO/PZT/Co junction, the initial voltage does change the MR, but there is still no shift of the $MR(V_{MR})$ function, because the dipole of PZT is expected to be screened by the metal electrodes. The change of MR in the LSMO/PZT/Co junction is more likely caused by the change of electronic structure at the interface due to the atomic displacement of the FE rather than the shift of vacuum potentials [24].

Dramatic changes were observed in the magneto transport of the LSMO/PZT/Alq_3/Co junction, after a larger electric field that switches the FE polarization of PZT was applied. First, the sign of $MR(V_{MR})$ function changes from all negative in the LSMO/PZT/Alq_3/Co junction with as grown PZT (polarization pointing up toward Alq_3) [Fig. 6(a)], to mostly positive after the FE polarization is switched to pointing down toward LSMO [Fig. 6(c)]. Second, the effect of V_{MAX} is not a simple shift of the $MR(V_{MR})$ function; instead, it may change the sign of the MR. The dependence of the MR sign on V_{MR} and V_{MAX} is in line with varying the polarization of PZT in minor polarization-voltage loop. It appears that, when the polarization is lower than a certain value, the MR becomes positive, as illustrated in Fig. 6(b). This dependence of MR sign on the polarization of PZT can be understood using the change of energy alignment between LSMO and Alq_3 due to the dipole moment of PZT. As shown in Fig. 6(d), due to the poor screening ability of Alq_3, the electric dipole moment of PZT generates a shift of the vacuum potential. When the PZT polarization is pointing up, the injection and collection of holes at the LSMO/PZT/Alq_3 interface is between the spin majority band of LSMO and Alq_3 HOMO. In contrast, when the PZT polarization is pointing down, the HOMO of Alq_3 is shifted up. The higher energy states of LSMO with minority spin becomes accessible for the injection and collection of holes at the LSMO/PZT/

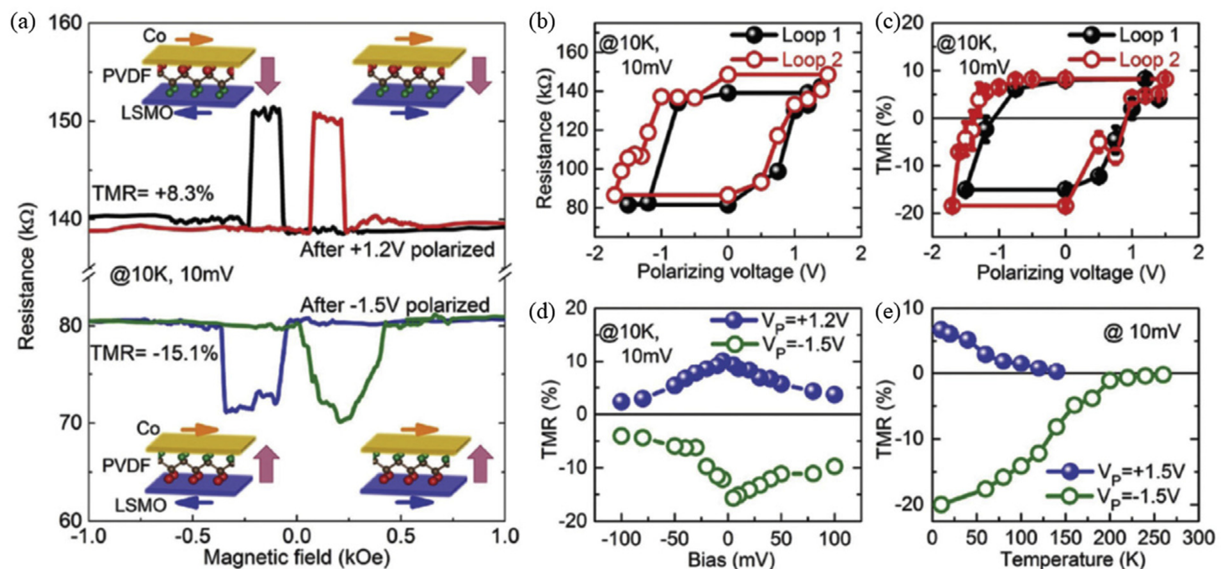

Fig. 7. MR of the LSMO/PVDF/Co junction. (a) MR measured when the PVDF polarization is pointing toward Co and toward LSMO respectively. (b) Resistance of the LSMO/PVDF/Co junction as a function of the poling voltage. (c) Tunneling MR as a function of the poling voltage. (d) Tunneling MR as a function of measurement voltage for 1.2 and −1.5 V poling voltages respectively. (e) Tunneling MR as a function of temperature for 1.5 and −1.5 V poling voltages respectively. Reproduced with permission from Ref. [34]. Copyright 2016, Wiely.

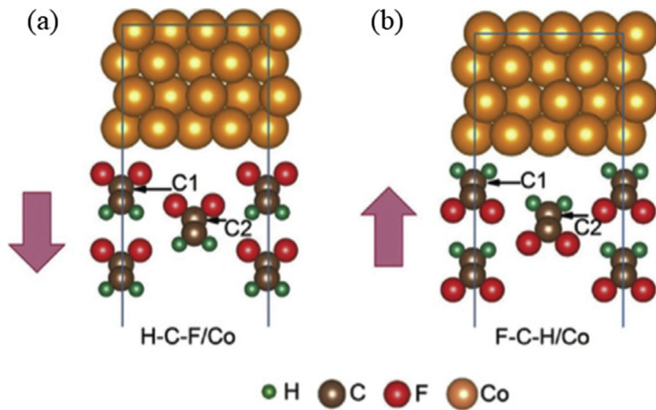

Fig. 8. Crystal structure at the Co/PVDF interface when the polarization is pointing away (a) and toward (b) Co respectively. Reproduced with permission from Ref. [34]. Copyright 2016, Wiley.

Alq_3 interface. Therefore, the shift of energy states in $A1q_3$ by the PZT dipole, may change the sign of interfacial spin polarization P^*, which changes the sign of the MR of the LSMO/PZT/Alq_3 junction.

6.2. Tunneling organic spin valves and the interfacial crystal structure

The effect of FE tunneling barrier in organic spin valves has been investigated by Liang et al. in LSMO/PVDF/Co junctions [34] [103]. The ferroelectricity of PVDF originates from the long-range order of the dipoles in the polymer and the switching corresponds to the collective rotation of dipoles along the molecular chains. As shown in Fig. 7(a), when the electric polarization of PVDF is switched to pointing down toward LSMO, the MR is positive. In contrast, when the polarization is pointing up toward Co, the MR is negative. In addition to MR, the resistance of the junction also changes significantly due to the reversal of polarization of PVDF. As shown in Fig. 7(b), the relation between the initial voltage and the resistance measured at a low voltage (10 mV), is plotted. A clear hysteresis is observed; the change of resistance due to the initial voltage is up to 75%. At the same time, the MR also shows a hysteretic behavior with respect to the initial voltage [Fig. 7(c)]. It appears that the direction of the electric polarization is correlated with the sign of MR, although the magnitude of the MR is larger when the electric polarization is pointing up toward Co. The asymmetry in the MR is also observed in the bias voltage dependence [Fig. 7(d)] and temperature dependence [Fig. 7(e)].

The dependence of MR on the initial voltage and the asymmetry in magnitude is explained in terms of the change of electronic structure at the PVDF/Co interface caused by the reversal of electric polarization of PVDF. As mentioned above, the reversal of electric polarization of PVDF corresponds to the rotation of the molecular dipole along the polymer chain. When the electric polarization is pointing toward Co, it is the hydrogen (H) atoms that are in direct contact with the Co. Otherwise, when the electric polarization is pointing toward LSMO, it is the fluorine (F) atoms that are at the Co/PVDF interface. Therefore, the structure of the PVDF/Co interface can be switched between H-C-F/Co and F-C-H/Co correspond to the FE polarization pointing to LSMO and Co respectively [Fig. 8(a) and (b)]. The density of states of PVDF at the PVDF/Co interface has been calculated. Since these states are gap states induced by the interface with Co, whether F or H atom are in direct contact with Co makes a significant difference. It was found that at the H-C-F/Co interface, although the spin polarization of the gap states of the first layer of PVDF is negative (the same sign as that in Co), the second layer gap states show a positive spin polarization. For the F-C-H/Co interface, both the first and second layer in PVDF show negative spin polarization for the gap states. These results explain the reversal of MR sign when the electric polarization of PVDF is reversed. In addition, it was found that the F-C-H/Co interface is more energetically stable than the H-C-F/Co interface, which is consistent with the observation that MR vanishes at lower temperature when the polarization is pointing toward LSMO (H-C-F/Co interface) than that when the polarization is pointing toward Co (F-C-H/Co interface) [Fig. 7(e)].

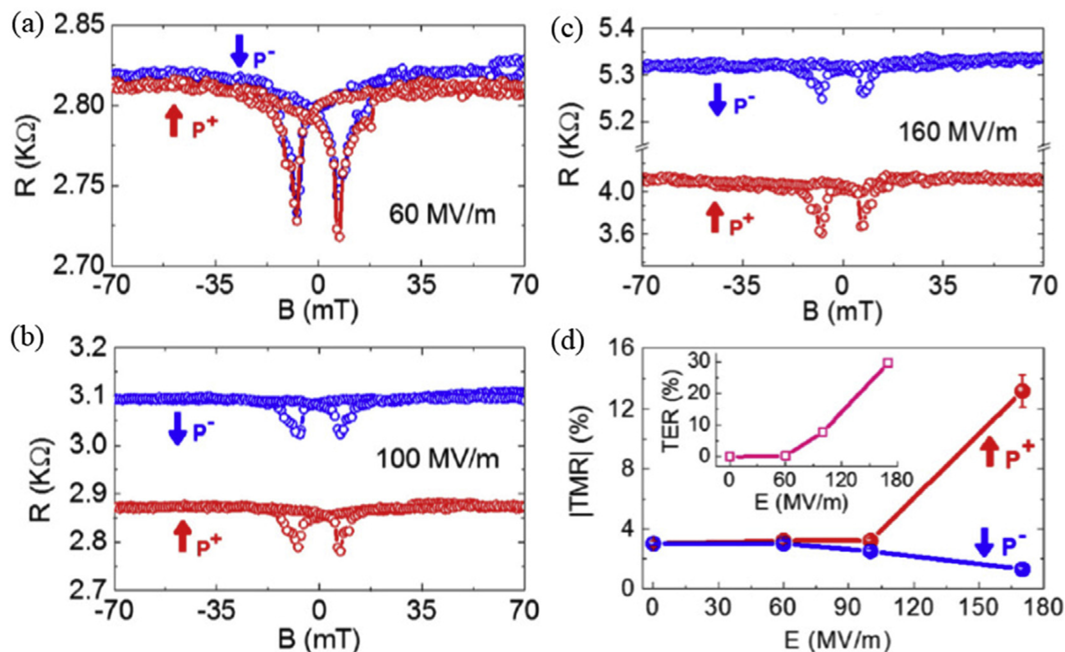

Fig. 9. MR of the LSMO/P(VDF-TrFE)/Co junction. (a)–(c) MR for positively and negatively poled P(VDF-TrFE) using 60, 100, and 160 MV/m respectively. (d) Tunneling MR and tunneling electroresistance (ER) as a function of poling fields. Reproduced with permission from Ref. [33]. Copyright 2017, the American Institute of Physics.

The effect of FE polarization on tunneling FM/FE/FM junction was also studied in LSMO/P(VDF-TrFE)/Co junctions at 200 K, where P(VDF-TrFE) stands for FE copolymers poly(vinylindene fluoride-trifluoroethylene) [33]. As shown in Fig. 9(a)-(c), the tunneling resistance of the junction depends on both the magnetic field and the initial pulsed electric field. The effect of the electric field increases with the magnitude of the field, consistent with the behavior of effect of electric field on the electric polarization. The effect of the electric field on MR also increases with the field, as shown in Fig. 9(d). Although the MR sign does not change when the electric polarization of the FE reverses, the asymmetry agrees with the previous results in the LSMO/PVDF/Co junctions [34]. Similar to that in the LSMO/PVDF/Co junctions, when the electric polarization is pointing up toward Co, a negative MR with larger magnitude is observed. When the electric polarization is pointing down toward LSMO, the sign of MR remains negative, but the magnitude decreases significantly. These results are consistent with the modification of interfacial state and the different coupling between the FE spacer and FM electrode when the electric polarization is switched.

7. Conclusion and outlook

The recent efforts of exploiting FE control of MR in organic spin valves show encouraging indication of effects on the energy alignment and on the interfacial crystal structures. However, since the exact mechanism of spin transport through organic spin valves is still not fully understood, more work on similar devices with other FE materials [103,106,107] and more characterization on the interfacial crystal structures and on the interfacial electronic structures are needed to elucidate the FE effect as well as other concomitant effects such as the change of magnetism of the electrodes [99,108,109] and change of transport mechanism [110–112]. At the same time, as the field of organic spintronics keeps growing, the spin polarization at the FM/organic interfaces (spinterface) will remain a focus. More examples of tuning the spinterface by varying the energy level alignment or by varying the interfacial crystal structure are expected to be investigated. These investigations will be not only important for organic spintronics; they will also be useful for tuning other electronic devices (such as light emission diode and photovoltaics) involving organic/inorganic interfaces.

Acknowledgements

This project was primarily supported by the National Science Foundation through the Nebraska Materials Research Science and Engineering Center (Grant No. DMR-1420645).

References

[1] Fert A. Nobel Lecture: origin, development, and future of spintronics. Rev Mod Phys 2008;80:1517–30. https://doi.org/10.1103/RevModPhys.80.1517.
[2] Sato K, Saitoh E. Spintronics for next generation innovative devices. Chichester, West Sussex, United Kingdom: John Wiley & Sons Ltd; 2016.
[3] Žutić I, Fabian J, Das Sarma S. Spintronics: fundamentals and applications. Rev Mod Phys 2004;76:323–410. https://doi.org/10.1103/RevModPhys.76.323.
[4] Gregg JF, Petej I, Jouguelet E, Dennis C. Spin electronics a review. J Phys D Appl Phys 2002;35:R121–55. https://doi.org/10.1088/0022-3727/35/18/201.
[5] Prinz G a. Spin-polarized transport. Phys Today 1995;48:58. https://doi.org/10.1063/1.881459.
[6] Dieny B, Speriosu VS, Parkin SSP, Gurney BA, Wilhoit DR, Mauri D. Giant magnetoresistance in soft ferromagneticmultilayers. Phys Rev B 1991;43:1297.
[7] Baibich MN, Broto JM, Fert A, Van Dau FN, Petroff F, Eitenne P, et al. Giant magnetoresistance of (001)Fe/(001)Cr magnetic superlattices. Phys Rev Lett 1988;61:2472–5. https://doi.org/10.1103/PhysRevLett.61.2472.
[8] Baibich MN, Broto JM, Fert A, Dau FN, Van Petroff F. Giant magnetoresistance of (001)Fel(001) Cr magnetic snperlattices. Phys Rev Lett 1988;61:2472–5.
[9] Binasch G, Griinberg P, Saurenbach F, Zinn W. Enhanced magnetoresistance in layered magnetic structures. Phys Rev B 1989;39:4828–30.
[10] Schad R, Potter CD, Beliën P, Verbanck G, Moshchalkov VV, Bruynseraede Y. Giant magnetoresistance in Fe/Cr superlattices with very thin Fe layers. Appl Phys Lett 1994;64:3500–2. https://doi.org/10.1063/1.111253.
[11] Piraux L, George JM, Despres JF, Leroy C, Ferain E, Legras R, et al. Giant magnetoresistance in magnetic multilayered nanowires. Appl Phys Lett 1994;65:2484–6. https://doi.org/10.1063/1.112672.
[12] Parkin SSP, More N, Roche KP. Oscillations in exchange coupling and magnetoresistance in metallic superlattice structures: Co/Ru, Co/Cr, and Fe/Cr. Phys Rev Lett 1990;64:2304–8.
[13] Parkin SSP, Bhadra R, Roche KP. Oscillatory magnetic exchange coupling through thin copper layers. Phys Rev Lett 1991;66:2152–5.
[14] Rashba EI. Theory of electrical spin injection: tunnel contacts as a solution of the conductivity mismatch problem. Phys Rev B 2000;62:267–70. https://doi.org/10.1103/PhysRevB.62.R16267.
[15] Fert A, Jaffrès H. Conditions for efficient spin injection from a ferromagnetic metal into a semiconductor. Phys Rev B 2001;64:184420. https://doi.org/10.1103/PhysRevB.64.184420.
[16] Smith DL, Silver RN. Electrical spin injection into semiconductors. Phys Rev B 2001;64:45323. https://doi.org/10.1103/PhysRevB.64.045323.
[17] Albrecht JD, Smith DL. Electron spin injection at a Schottky contact. Phys Rev B 2002;66:113303. https://doi.org/10.1103/PhysRevB.66.113303.
[18] Pramanik S, Stefanita C-G, Patibandla S, Bandyopadhyay S, Garre K, Harth N, et al. Observation of extremely long spin relaxation times in an organic nanowire spin valve. Nat Nanotechnol 2007;2:216–9.
[19] McCamey DR, Seipel HA, Paik S-Y, Walter MJ, Borys NJ, Lupton JM, et al. Spin Rabi flopping in the photocurrent of a polymer light-emitting diode. Nat Mater 2008;7:723–8.
[20] Xiong ZH, Wu D, Valy Vardeny Z, Shi J. Giant magnetoresistance in organic spin-valves. Nature 2004;427:821–4.
[21] Dediu V, Murgia M, Matacotta FC, Taliani C, Barbanera S. Room temperature spin polarized injection in organic semiconductor. Solid State Commun 2002;122:181–4. https://doi.org/10.1016/S0038-1098(02)00090-X.
[22] Sanvito S. Molecular spintronics: the rise of spinterface science. Nat Phys 2010;6:562–4. https://doi.org/10.1038/nphys1714.
[23] Zhuravlev MY, Jaswal SS, Tsymbal EY, Sabirianov RF. Ferroelectric switch for spin injection. Appl Phys Lett 2005;87:222114. https://doi.org/10.1063/1.2138365.
[24] Pantel D, Goetze S, Hesse D, Alexe M. Reversible electrical switching of spin polarization in multiferroic tunnel junctions. Nat Mater 2012;11:289–93.
[25] Tsymbal EY. Applied physics: tunneling across a ferroelectric. Science 2006;313:181–3. https://doi.org/10.1126/science.1126230.
[26] Jang H-J, Pernstich KP, Gundlach DJ, Jurchescu OD, Richter CA. Observation of spin-polarized electron transport in Alq3 by using a low work function metal. Appl Phys Lett 2012;101:102412. https://doi.org/10.1063/1.4751257.
[27] Jiang SW, Chen BB, Wang P, Zhou Y, Shi YJ, Yue FJ, et al. Voltage polarity manipulation of the magnetoresistance sign in organic spin valve devices. Appl Phys Lett 2014;104:262402. https://doi.org/10.1063/1.4885770.
[28] Jang H-J, Richter CA. Organic spin-valves and beyond: spin injection and transport in organic semiconductors and the effect of interfacial engineering. Adv Mater 2017;29:1602739. https://doi.org/10.1002/adma.201602739.
[29] Zhan Y, Holmström E, Lizárraga R, Eriksson O, Liu X, Li F, et al. Efficient spin injection through exchange coupling at organic semiconductor/ferromagnet heterojunctions. Adv Mater 2010;22:1626–30. https://doi.org/10.1002/adma.200903556.
[30] Campbell IH, Kress JD, Martin RL, Smith DL, Barashkov NN, Ferraris JP. Controlling charge injection in organic electronic devices using self-assembled monolayers. Appl Phys Lett 1997;71:3528–30. https://doi.org/10.1063/1.120381.
[31] Lukashev PV, Paudel TR, López-Encarnación JM, Adenwalla S, Tsymbal EY, Velev JP. Ferroelectric control of magnetocrystalline anisotropy at cobalt/poly(vinylidene fluoride) interfaces. ACS Nano 2012;6:9745–50. https://doi.org/10.1021/nn303212h.
[32] Cui B, Song C, Mao H, Wu H, Li F, Peng J, et al. Magnetoelectric coupling induced by interfacial orbital reconstruction. Adv Mater 2015;27:6651–6. https://doi.org/10.1002/adma.201503115.
[33] Subedi RC, Geng R, Luong HM, Huang W, Li X, Hornak LA, et al. Large magnetoelectric effect in organic ferroelectric copolymer-based multiferroic tunnel junctions. Appl Phys Lett 2017;110:53302. https://doi.org/10.1063/1.4974490.
[34] Liang S, Yang H, Yang H, Tao B, Djeffal A, Chshiev M, et al. Ferroelectric control of organic/ferromagnetic spinterface. Adv Mater 2016;28:10204–10. https://doi.org/10.1002/adma.201603638.
[35] Sun D, Fang M, Xu X, Jiang L, Guo H, Wang Y, et al. Active control of magnetoresistance of organic spin valves using ferroelectricity. Nat Commun 2014;5:4396. https://doi.org/10.1038/ncomms5396.
[36] López-Encarnación JM, Burton JD, Tsymbal EY, Velev JP. Organic multiferroic tunnel junctions with ferroelectric poly(vinylidene fluoride) barriers. Nano Lett 2011;11:599–603. https://doi.org/10.1021/nl103650b.
[37] Son PC, van Kempen H, van Wyder P. Boundary resistance of the ferromagnetic-nonferromagnetic metal interface. Phys Rev Lett 1987;58:2271.
[38] Johnson M, Silsbee RH. Interfacial charge-spin coupling: injection and detection of spin magnetization in metals. Phys Rev Lett 1985;55:1790–3. https://doi.org/10.1103/PhysRevLett.55.1790.
[39] Bass J, Pratt WP. Spin-diffusion lengths in metals and alloys, and spin-

flipping at metal/metal interfaces: an experimentalist's critical review. J Phys Condens Matter 2007;19:183201. https://doi.org/10.1088/0953-8984/19/18/183201.

[40] Elliott RJ. Theory of the effect of spin-orbit coupling on magnetic resonance in Some semiconductors. Rev Mod Phys 1954;96:266.

[41] Vinet L, Zhedanov AA. "missing" family of classical orthogonal polynomials. Phys Rev B 2010;48:7099–113. https://doi.org/10.1088/1751-8113/44/8/085201.

[42] De Teresa J, Barthélémy A, Fert A, Contour J, Lyonnet R, Montaigne F, et al. Inverse tunnel magnetoresistance in Co/$SrTiO_3$/$La_{0.7}Sr_{0.3}MnO_3$: new ideas on spin-polarized tunneling. Phys Rev Lett 1999;82:4288–91. https://doi.org/10.1103/PhysRevLett.82.4288.

[43] Park J-H, Vescovo E, Kim H-J, Kwon C, Ramesh R, Venkatesan T. Magnetic properties at surface boundary of a half-metallic ferromagnet La0.7Sr0.3MnO3. Phys Rev Lett 1998;81:1953–6.

[44] Schmidt G, Ferrand D, Molenkamp L, Filip a, van Wees B. Fundamental obstacle for electrical spin injection from a ferromagnetic metal into a diffusive semiconductor. Phys Rev B 2000;62:R4790–3. https://doi.org/10.1103/PhysRevB.62.R4790.

[45] Julliere M. Tunneling between ferromagnetic films. Phys Lett A 1975;54:225–6. https://doi.org/10.1016/0375-9601(75)90174-7.

[46] Ikeda S, Hayakawa J, Ashizawa Y, Lee YM, Miura K, Hasegawa H, et al. Tunnel magnetoresistance of 604% at 300 K by suppression of Ta diffusion in CoFeBMgOCoFeB pseudo-spin-valves annealed at high temperature. Appl Phys Lett 2008;93:2006–9. https://doi.org/10.1063/1.2976435.

[47] De Teresa JM. Role of metal-oxide interface in determining the spin polarization of magnetic tunnel junctions. Science 1999;286:507–9. https://doi.org/10.1126/science.286.5439.507.

[48] Santos TS, Lee JS, Migdal P, Lekshmi IC, Satpati B, Moodera JS. Room-temperature tunnel magnetoresistance and spin-polarized tunneling through an organic semiconductor barrier. Phys Rev Lett 2007;98:16601.

[49] Xu W, Szulczewski GJ, LeClair P, Navarrete I, Schad R, Miao G, et al. Tunneling magnetoresistance observed in La0.67Sr0.33MnO3/organic molecule/Co junctions. Appl Phys Lett 2007;90:72506. https://doi.org/10.1063/1.2435907.

[50] Vinzelberg H, Schumann J, Elefant D, Gangineni RB, Thomas J, Büchner B. Low temperature tunneling magnetoresistance on (La,Sr)MnO3;Co junctions with organic spacer layers. J Appl Phys 2008;103:93720. https://doi.org/10.1063/1.2924435.

[51] Szulczewski G, Tokuc H, Oguz K, Coey JMD. Magnetoresistance in magnetic tunnel junctions with an organic barrier and an MgO spin filter. Appl Phys Lett 2009;95:202506. https://doi.org/10.1063/1.3264968.

[52] Barraud C, Seneor P, Mattana R, Fusil S, Bouzehouane K, Deranlot C, et al. Unravelling the role of the interface for spin injection into organic semiconductors. Nat Phys 2010;6:615–20. https://doi.org/10.1038/nphys1688.

[53] Liang SH, Liu DP, Tao LL, Han XF, Guo H. Organic magnetic tunnel junctions: the role of metal-molecule interface. Phys Rev B 2012;86:224419. https://doi.org/10.1103/PhysRevB.86.224419.

[54] Schoonus JJHM, Lumens PGE, Wagemans W, Kohlhepp JT, Bobbert PA, Swagten HJM, et al. Magnetoresistance in hybrid organic spin valves at the onset of multiple-Step tunneling. Phys Rev Lett 2009;103:146601.

[55] Wang FJ, Yang CG, Vardeny ZV, Li XG. Spin response in organic spin valves based on La2/3Sr1/3MnO3 electrodes. Phys Rev B 2007;75:245324. https://doi.org/10.1103/PhysRevB.75.245324.

[56] Dediu V, Hueso LE, Bergenti I, Riminucci A, Borgatti F, Graziosi P, et al. Room-temperature spintronic effects in Alq3-based hybrid devices. Phys Rev B 2008;78:115203.

[57] Yoo J-W, Jang HW, Prigodin VN, Kao C, Eom CB, Epstein AJ. Giant magnetoresistance in ferromagnet/organic semiconductor/ferromagnet heterojunctions. Phys Rev B 2009;80:205207. https://doi.org/10.1103/PhysRevB.80.205207.

[58] Sun D, Yin L, Sun C, Guo H, Gai Z, Zhang X-G, et al. Giant magnetoresistance in organic spin valves. Phys Rev Lett 2010;104:236602.

[59] Nguyen TD, Hukic-Markosian G, Wang F, Wojcik L, Li X-G, Ehrenfreund E, et al. Isotope effect in spin response of π-conjugated polymer films and devices. Nat Mater 2010;9:345–52. https://doi.org/10.1038/nmat2633.

[60] Li F, Li T, Chen F, Zhang F. Excellent spin transport in spin valves based on the conjugated polymer with high carrier mobility. Sci Rep 2015;5:9355. https://doi.org/10.1038/srep09355.

[61] Geng R, Daugherty TT, Do K, Luong HM, Nguyen TD. A review on organic spintronic materials and devices: II. Magnetoresistance in organic spin valves and spin organic light emitting diodes. J Sci Adv Mater Devices 2016;1:256–72. https://doi.org/10.1016/j.jsamd.2016.05.002.

[62] Devkota J, Geng R, Subedi RC, Nguyen TD. Organic spin valves: a review. Adv Funct Mater 2016;26:3881–98. https://doi.org/10.1002/adfm.201504209.

[63] Johnson M, Silsbee RH. Spin injection experiment. Phys Rev B 1988;37:5326.

[64] Jedema FJ, Heersche HB, Filip AT, Baselmans JJA, van Wees BJ. Electrical detection of spin precession in a metallic mesoscopic spin valve. Nature 2002;416:713–6. https://doi.org/10.1038/416713a.

[65] Crooker SA, Furis M, Lou X, Adelmann C, Smith DL, Palmstrøm CJ, et al. Imaging spin transport in lateral ferromagnet/semiconductor structures. Science 2005;309:2191–5. https://doi.org/10.1126/science.1116865.

[66] Lou X, Adelmann C, Furis M, Crooker SA, Palmstrøm CJ, Crowell PA. Electrical detection of spin accumulation at a ferromagnet-semiconductor interface. Phys Rev Lett 2006;96:176603. https://doi.org/10.1103/PhysRevLett.96.176603.

[67] van 't Erve OMJ, Hanbicki AT, Holub M, Li CH, Awo-Affouda C, Thompson PE, et al. Electrical injection and detection of spin-polarized carriers in silicon in a lateral transport geometry. Appl Phys Lett 2007;91:212109. https://doi.org/10.1063/1.2817747.

[68] Huang B, Monsma DJ, Appelbaum I. Coherent spin transport through a 350 micron thick silicon wafer. Phys Rev Lett 2007;99:177209. https://doi.org/10.1103/PhysRevLett.99.177209.

[69] Appelbaum I, Huang B, Monsma DJ. Electronic measurement and control of spin transport in silicon. Nature 2007;447:295–8. https://doi.org/10.1038/nature05803.

[70] Huang B, Monsma DJ, Appelbaum I. Experimental realization of a silicon spin field-effect transistor. Appl Phys Lett 2007;91:72501. https://doi.org/10.1063/1.2770656.

[71] Huang B, Jang H-J, Appelbaum I. Geometric dephasing-limited Hanle effect in long-distance lateral silicon spin transport devices. Appl Phys Lett 2008;93:162508. https://doi.org/10.1063/1.3006333.

[72] Jang H-J, Appelbaum I. Spin polarized electron transport near the Si/SiO2 interface. Phys Rev Lett 2009;103:117202. https://doi.org/10.1103/PhysRevLett.103.117202.

[73] Lu Y, Appelbaum I. Reverse Schottky-asymmetry spin current detectors. Appl Phys Lett 2010;97:162501. https://doi.org/10.1063/1.3504659.

[74] Lu Y, Li J, Appelbaum I. Spin-polarized transient electron trapping in phosphorus-doped silicon. Phys Rev Lett 2011;106:217202. https://doi.org/10.1103/PhysRevLett.106.217202.

[75] Riminucci A, Prezioso M, Pernechele C, Graziosi P, Bergenti I, Cecchini R, et al. Hanle effect missing in a prototypical organic spintronic device. Appl Phys Lett 2013;102:92407. https://doi.org/10.1063/1.4794408.

[76] Schulz L, Nuccio L, Willis M, Desai P, Shakya P, Kreouzis T, et al. Engineering spin propagation across a hybrid organic/inorganic interface using a polar layer. Nat Mater 2011;10:39–44. https://doi.org/10.1038/nmat2912.

[77] Drew AJ, Hoppler J, Schulz L, Pratt FL, Desai P, Shakya P, et al. Direct measurement of the electronic spin diffusion length in a fully functional organic spin valve by low-energy muon spin rotation. Nat Mater 2009;8:109–14. https://doi.org/10.1038/nmat2333.

[78] Cinchetti M, Heimer K, Wüstenberg J-P, Andreyev O, Bauer M, Lach S, et al. Determination of spin injection and transport in a ferromagnet/organic semiconductor heterojunction by two-photon photoemission. Nat Mater 2009;8:115–9. https://doi.org/10.1038/nmat2334.

[79] Watanabe S, Ando K, Kang K, Mooser S, Vaynzof Y, Kurebayashi H, et al. Polaron spin current transport in organic semiconductors. Nat Phys 2014;10:308–13. https://doi.org/10.1038/nphys2901.

[80] Schuller JA, Karaveli S, Schiros T, He K, Yang S, Kymissis I, et al. Orientation of luminescent excitons in layered nanomaterials. Nat Nanotechnol 2013;8:271–6. https://doi.org/10.1038/nnano.2013.20.

[81] Yoo JW, Jang HW, Prigodin VN, Kao C, Eom CB, Epstein AJ. Tunneling vs. giant magnetoresistance in organic spin valve. Synth Met 2010;160:216–22. https://doi.org/10.1016/j.synthmet.2009.11.019.

[82] Morley NA, Rao A, Dhandapani D, Gibbs MRJ, Grell M, Richardson T. Room temperature organic spintronics. J Appl Phys 2008;103:07F306. https://doi.org/10.1063/1.2829245.

[83] Jiang JS, Pearson JE, Bader SD. Absence of spin transport in the organic semiconductor Alq3. Phys Rev B 2008;77:35303. https://doi.org/10.1103/PhysRevB.77.035303.

[84] Tagantsev AK, Gerra G. Interface-induced phenomena in polarization response of ferroelectric thin films. J Appl Phys 2006;100:51607. https://doi.org/10.1063/1.2337009.

[85] Tessler N, Preezant Y, Rappaport N, Roichman Y. Charge transport in disordered organic materials and its relevance to thin-film devices: a tutorial review. Adv Mater 2009;21:2741–61. https://doi.org/10.1002/adma.200803541.

[86] Baldo MA, Forrest SR. Interface-limited injection in amorphous organic semiconductors. Phys Rev B 2001;64:85201. https://doi.org/10.1103/PhysRevB.64.085201.

[87] Chiu FA. Review on conduction mechanisms in dielectric films. Adv Mater Sci Eng 2014;2014:578168. https://doi.org/10.1155/2014/578168.

[88] Roundy RC, Raikh ME. Spin transport with dispersive traps: narrowing of the Hanle curve. Phys Rev B 2014;90:241202. https://doi.org/10.1103/PhysRevB.90.241202.

[89] Yu ZG. Suppression of the Hanle effect in organic spintronic devices. Phys Rev Lett 2013;111:16601. https://doi.org/10.1103/PhysRevLett.111.016601.

[90] Jiang SW, Liu S, Wang P, Luan ZZ, Tao XD, Ding HF, et al. Exchange-dominated pure spin current transport in Alq3 molecules. Phys Rev Lett 2015;115:86601. https://doi.org/10.1103/PhysRevLett.115.086601.

[91] Zhan YQ, Liu XJ, Carlegrim E, Li FH, Bergenti I, Graziosi P, et al. The role of aluminum oxide buffer layer in organic spin-valves performance. Appl Phys Lett 2009;94:53301. https://doi.org/10.1063/1.3078274.

[92] Li B, Kao CY, Yoo JW, Prigodin VN, Epstein AJ. Magnetoresistance in an all-organic-based spin valve. Adv Mater 2011;23:3382–6. https://doi.org/10.1002/adma.201100903.

[93] Lines ME, Glass AM. Principles and applications of ferroelectrics and related materials. Oxford [Eng.]: Clarendon Press; 1977.

[94] Zhuravlev MY, Sabirianov RF, Jaswal SS, Tsymbal EY. Giant electroresistance in ferroelectric tunnel junctions. Phys Rev Lett 2005;94:246802. https://doi.org/10.1103/PhysRevLett.94.246802.

[95] Yeo YC, King TJ, Hu C. Metal-dielectric band alignment and its implications

for metal gate complementary metal-oxide-semiconductor technology. J Appl Phys 2002;92:7266–71. https://doi.org/10.1063/1.1521517.
[96] Campbell IH, Smith DL. Schottky energy barriers and charge injection in metal/alq/metal structures. Appl Phys Lett 1999;74:561–3. https://doi.org/10.1063/1.123145.
[97] Zhan YQ, de Jong MP, Li FH, Dediu V, Fahlman M, Salaneck WR. Energy level alignment and chemical interaction at Alq3/Co interfaces for organic spintronic devices. Phys Rev B 2008;78:45208.
[98] Grobosch M, Dörr K, Gangineni RB, Knupfer M. Energy level alignment and injection barriers at spin injection contacts between La0.7Sr0.3MnO3 and organic semiconductors. Appl Phys Lett 2008;92:23302. https://doi.org/10.1063/1.2829391.
[99] Lu H, George TA, Wang Y, Ketsman I, Burton JD, Bark C-W, et al. Electric modulation of magnetization at the BaTiO3/La0. 67Sr0. 33MnO3 interfaces. Appl Phys Lett 2012;100:232904. https://doi.org/10.1063/1.4726427.
[100] Garcia V, Bibes M, Bocher L, Valencia S, Kronast F, Crassous A, et al. Ferroelectric control of spin polarization. Science 2010;327:1106–10. https://doi.org/10.1126/science.1184028.
[101] Valencia S, Crassous A, Bocher L, Garcia V, Moya X, Cherifi RO, et al. Interface-induced room-temperature multiferroicity in BaTiO3. Nat Mater 2011;10:753–8.
[102] Velev JP, López-Encarnación JM, Burton JD, Tsymbal EY. Multiferroic tunnel junctions with poly(vinylidene fluoride). Phys Rev B 2012;85:125103. https://doi.org/10.1103/PhysRevB.85.125103.
[103] Horiuchi S, Tokura Y. Organic ferroelectrics. Nat Mater 2008;7:357–66. https://doi.org/10.1038/nmat2137.
[104] Lide DR. CRC handbook of chemistry and physics: a ready-reference book of chemical and physical data. Boca Raton, FL: CRC Press; 1994.
[105] Lee HN, Nakhmanson SM, Chisholm MF, Christen HM, Rabe KM, Vanderbilt D. Suppressed dependence of polarization on epitaxial Strain in highly polar ferroelectrics. Phys Rev Lett 2007;98:217602. https://doi.org/10.1103/PhysRevLett.98.217602.
[106] Horiuchi S, Tokunaga Y, Giovannetti G, Picozzi S, Itoh H, Shimano R, et al. Above-room-temperature ferroelectricity in a single-component molecular crystal. Nature 2010;463:789–92. https://doi.org/10.1038/nature09363.
[107] Jiang X, Lu H, Yin Y, Zhang X, Wang X, Yu L, et al. Room temperature ferroelectricity in continuous croconic acid thin films Room temperature ferroelectricity in continuous croconic acid thin films. Appl Phys Lett 2016;109:102902. https://doi.org/10.1063/1.4962278.
[108] Burton JD, Tsymbal EY. Prediction of electrically induced magnetic reconstruction at the manganite/ferroelectric interface. Phys Rev B 2009;80:174406.
[109] Meyer TL, Herklotz A, Lauter V, Freeland JW, Nichols J, Guo EJ, et al. Enhancing interfacial magnetization with a ferroelectric. Phys Rev B 2016;94:174432. https://doi.org/10.1103/PhysRevB.94.174432.
[110] Yu ZG. Impurity-band transport in organic spin valves. Nat Commun 2014;5:4842. https://doi.org/10.1038/ncomms5842.
[111] Hueso LE, Bergenti I, Riminucci A, Zhan Y, Dediu V. Multipurpose magnetic organic hybrid devices. Adv Mater 2007;19:2639–42. https://doi.org/10.1002/adma.200602748.
[112] Prezioso M, Riminucci A, Bergenti I, Graziosi P, Brunel D, Dediu VA. Electrically Programmable magnetoresistance in multifunctional organic-based spin valve devices. Adv Mater 2011;23:1371–5. https://doi.org/10.1002/adma.201003974.

Professor Xiaoshan Xu, University of Nebraska-LincolnDr. Xiaoshan Xu is an assistance professor in the Department of Physics and Astronomy in University of Nebraska-Lincoln. Before joining the faculty of University of Nebraska-Lincoln in 2013, he worked as a research staff member at Oak Ridge National Lab and as a postdoctoral researcher in University of Tennessee. His current research focus is on multiferroic oxide thin films and organic/inorganic interfaces. Dr. Xu is a recipient of the Eugene P. Wigner Fellowship in the Oak Ridge National Lab and the Faculty Early Career Development Award from the National Science Foundation.